Journal of Hydroscience and Hydraulic Engineering
Vol. 27, No.1 May, 2009, 89-103

NUMERICAL CALCULATION OF THREE-DIMENSIONAL FLOWS IN AN OPEN CHANNEL WITH A RUBBLE MOUND GROIN BY USING NON-DARCIAN RESISTANCE LAW

By

Ryosuke Akahori

Graduate School of Science and Engineering, Tokyo Institute of Technology, Meguro-ku, Tokyo, Japan

and

Kohji Michioku

Graduate School of Engineering, Kobe University, Nada-ku, Kobe, Japan

SYNOPSIS

This study presents a combined numerical model of a porous flow model that adopts the non-Darcian resistance law and a 3-dimensional Large Eddy Simulation model in order to investigate three-dimensional and temporal structures of flows around a rubble mound groin. The model's accuracy is cross-checked by comparing the numerical results to the observed results of an existing experiment. The model's results show good agreement in terms of time- and depth-averaged sense. Calculation results also suggest that a permeable groin restricts growth of secondary flows in a constriction section. However, a combined model is not able to produce unsteady characteristics of flows that are caused by small scale and structured turbulences in a down-stream region of a groin.

INTRODUCTION

Recently, river management programs, whereby naturally derived permeable materials are used to develop river engineering structures, are frequently implemented in Japan. The reason for this is the rising of the public awareness of natural environments and the revision of the Japanese River Law in 1997. One example of these permeable structures is a rubble mound weir, which has been historically used as a water intake weir for agricultural purposes. Although rubble mound weirs have several environmental advantages compared with those made of impermeable materials, there are some difficulties in developing them, because of their vulnerability to floods. Planning with those permeable weirs thus needs appropriate design, execution, and management. These factors have been empirically treated. Current river management strategies, however, require rational criteria based on the hydraulic knowledge of permeable river structures, and an understanding of the characteristics of flows is necessary for popularization of nature-oriented river engineering methods.

Several previous researches on rubble mount weirs or groins have been carried out. Maeno et al. (1) illustrated

the gradual characteristic change of a weir under its destruction process by experiments, and Maeno et al. (2) succeeded in reproducing vertical 2-dimensional flow and water surface topography over a weir by employing the volume of fluid (VOF) method. Michioku et al. (3) examined hydraulic characteristics of porous media that consists of rubbles, such as the law of the resistance, by experimental and theoretical methods. Michioku et al. (4) proposed a depth-averaged two-layer model that is able to calculate open channels and porous medium flows simultaneously. The model shows good agreement with experimental results in terms of time- and depth-averaged senses.

Numerical analyses provide precise information that is difficult to obtain by experimental methods, such as interior flows of porous medium and shear flows around permeable obstacles. Numerical methods are thus useful in cases of evaluation of stress distributions and river-bed evolutions around hydraulic structures. However, the most of previous papers aforementioned focus on flow fields on a horizontal or a vertical 2-dimensional plane, hence they do not provide 3-dimensional flow information induced by river engineering structures, such as weirs or groins. Akahori (5) employs a 3-dimensional Large Eddy Simulation (LES) model to investigate the relations between secondary flows, which are generated in a main channel section near an impermeable groin, and horizontal large eddies, which are generated along a shear layer between the main channel and a downstream section of the groin. As a result, they find that such secondary flows influence on the intermittency of the generation of large eddies. Also, Nagata et al. (6) mentioned that the three-dimensional flows beside an impermeable dike plays a dominant role on the erosion process near an impermeable structure. From such results, it is possible to ascertain that the 3-dimensionality of flows around weirs or groins may also have an influence on sediment transport even in cases of structures are permeable. Unsteady and 3-dimensional numerical analyses are thereby required to make a rational investigation of characteristics of permeable river engineering structures on sediment transport.

Although the necessity of three-dimensional analysis, only a few methods to investigate such flows around permeable hydraulic structures have been proposed. The multi-phase flow model by Ushijima et al. (7) is one of such methods. This model directly calculates flows between porous medium by using the multi-phase model and the interaction between flows and particles by using the distinct element method. It is one of the most precise models in terms of reproducing physical mechanisms. Thus, it is ideal for investigating the process of collapse of permeable structures, such as rubble mound hydraulic structures. However, it may not be appropriate in some cases where investigating large scale flow structures is the main purpose because of its demanding characteristic which requires that each element is resolved by a calculation gird.

We propose a 3-dimensional unsteady numerical model for flows around a permeable structure by combining a LES model for open channel flows and a flow model with the non-Darcian resistance law for porous medium flows. Our model focuses on the latter purpose mentioned in the above paragraph. It is aimed to solve three-dimensional and large scale flow characteristics around permeable hydraulic structures. Flows in permeable structures are solved as spatially averaged form in this method (flows around distinct elements are not resolved by a calculation gird) and it requires some empirical values, such as drag coefficients. We thus expect to provide reasonable flow structures with the more simple procedure than the above mentioned method despite the fact that it is difficult to accurately reproduce small scale flow structures in permeable medium. The proposed model is applied to an open channel flow with a permeable rubble mound groin, and the flow characteristics and the applicability of this modeling technique are investigated.

NUMERICAL MODEL

In this study, the non-Darcian resistance law that is proposed to be used in the two-layer model by Michioku et al. (4) is also employed to calculate porous medium flows. This law is aimed to solve time-averaged flows in porous

medium in the work by Michioku et al. (4). However, it is not clear whether it applies to solving unsteady flows. Here, it is assumed that the non-Darcian resistance law model provides a sufficiently accurate time-averaged solution in a porous structure, and it is also assumed that the LES model can accurately resolve flow fields in an open section with the solution of porous flow by the non-Darcian model. When the primary purpose of calculations is to solve flows in open channel sections, this method is regarded as a practical approach.

The LES model in an open channel

For the open channel section, the three-dimensional Large Eddy Simulation (LES) model is employed. Here, the Smagorinsky model is used as the Sub-grid Scale (SGS) model (8). The spatially filtered basic equations, the continuity equation, Eq. 1, and the Navier-Stokes equations, Eq. 2 are expressed as follows:

$$\frac{\partial \overline{u_i}}{\partial x_i} = 0 \tag{1}$$

$$\frac{\partial \overline{u_i}}{\partial t} = -\frac{1}{\rho}\frac{\partial P}{\partial x_i} - \frac{\partial \left(\overline{u_i}\,\overline{u_j}\right)}{\partial x_j} + \frac{\partial}{\partial x_j}\left(2\nu_e \overline{S_{ij}}\right) + g_i \tag{2a}$$

$$\nu_e = \nu + \nu_t \tag{2b}$$

$$\nu_t = \left(C_s \Delta\right)^2 \left(2\overline{S_{ij}}\,\overline{S_{ij}}\right)^{\frac{1}{2}} \tag{2c}$$

$$\overline{S_{ij}} = \frac{1}{2}\left(\frac{\partial \overline{u_i}}{\partial x_j} + \frac{\partial \overline{u_j}}{\partial x_i}\right) \tag{2d}$$

where, over bar denotes spatially filtered value; i represents each component of grid system; u_i = flow velocity; x_i = axes of the grid system; t = time; ρ = fluid density; g_i = body force, ν = eddy viscosity; C_S = Smagorinsky coefficient; $\Delta = (\Delta x_1 \Delta x_2 \Delta x_3)^{1/3}$; Δx_i = grid scale; $P = p+2/3q$; p = pressure; and q = SGS kinetic energy.

In the actual calculation procedure in this study, these equations are transformed into the moving body fitted coordinate (BFC) system based on the same technique by Hosoda et al. (9), and the geometry of the free water surface that defines the moving boundary is obtained by the following equation, Eq. 3, which represents the kinematic boundary condition on the free surface.

$$\frac{\partial H}{\partial t} + u\frac{\partial H}{\partial x} + \upsilon\frac{\partial H}{\partial y} = w \tag{3}$$

Here, H = water level; u, v = horizontal components of flow velocity; w = vertical component of flow velocity; and x, y = horizontal component of the cartesian coordinate system. This kind of the free surface treatment requires that the water level must be a single-valued function. Thus, it cannot be applied to conditions where wave breaking is observed. Furthermore, the propagation speed of surface waves, which can be estimated by the small amplitude theory, restricts the period of the time step: the distance of the propagation in each time step must not exceed the distance between each grid cell. The calculation time step has to be sufficiently small to satisfy the above requirement.

In this model, the dumping effect of turbulence near the water surface is not specifically modeled. It needs to be considered in the future studies.

The porous media flow model with the non-Darcian resistance law

The basic equation for the porous medium flow, Eq. 4, is obtained by expanding the two-dimensional version by Michioku et al., which is based on the non-Darcian resistance law proposed by Ward et al. (10).

$$\frac{1}{n}\frac{\partial U_{si}}{\partial t} = -\frac{1}{\rho}\frac{\partial p}{\partial x_i} - \frac{1}{n^2}U_{si}\frac{\partial U_{sj}}{\partial x_j} + \frac{1}{n^2}\frac{\partial}{\partial x_j}\left(-\overline{u_{si}' u_{sj}'}\right) - \left(\frac{\nu}{K} + \frac{c}{\sqrt{K}}\sqrt{U_{sj}U_{sj}}\right)U_{si} \tag{4}$$

Here, subscript s = apparent velocity; $u_{si} = nu_i$; n = porosity; U = ensemble averaged velocity; u' = fluctuating value from the ensemble averaged value; and K, c = characteristic parameters of porous medium.

Inside the brackets of the third term on the right-hand side of Eq. 4 represents the Reynolds stress. The fourth term on the right-hand side represents the flow resistance in porous medium, and the first term inside the brackets represents the laminar flow resistance by Darcy's law, and the second term represents the resistance law of the turbulence, respectively. Michioku et al. (4) find that the fourth term on the right-hand side of equation (4) is dominant in porous media. The Reynolds stress by the third term is hence disregarded in the model of this study. K and c are given as follows:

$$\sqrt{K} = e\,d_m, \quad c = f\left(\frac{d_m}{\sqrt{K}/n}\right)^{-3/2} \tag{5}$$

in which, d_m = average diameter of particles of porous medium; and e, f = non-dimensionalized coefficient of particle shape. The proposed model for porous medium flow is based on the results by Michioku et al.(3), and the validity of the parameterization of K and c and the simplification for the turbulent flows were only confirmed under the conditions in their study. These configurations are expected to vary for different porous medium settings, hence need to be estimated again for each case. This is one of the limitations of this model.

The continuity equation for the porous medium flow is the same as Eq. 1, however it is applied for apparent flows rather than for real flow velocity components in void space of porous medium.

Calculation procedure

In calculations for the open channel section, the separation method, where the pressure term, the viscosity term, and the advection term are subsequently calculated, is employed, in order to use the CIP method (11) for the advection term. The pressure term is simultaneously calculated by using the continuity equation, Eq. 1, by the SMAC method and the water level by Eq. 3, iteratively. In the viscosity term calculation, the law of the wall is applied for boundaries with solid surfaces, except for walls of a permeable groin.

For the calculations of interior flows of porous media section, the separation method is again applied in order to

use the CIP method. In this section, the water level is calculated, where the level is set to satisfy the mass flux balance in one vertical column of grid cells, instead of using the kinematic boundary condition, Eq. 3, because the fluctuation of the water surface level is thought to be not so intense as that of the open channel section. The numerical technique for the water level calculation is the Runge-Kutta method, here.

Arrangements of unknown values in each cell follow the staggered grid system, and each component of velocity is set on boundaries of a cell. The interface between the open channel and porous medium sections is set on the boundary of cells, and the condition, which confirms that mass fluxes obtained by the normal flow velocity of the open channel section and by the normal apparent flow velocity of the porous medium section are equal on the boundary, is applied. This condition is used to simultaneously solve the pressure term and the continuity equation, Eq. 1, by means of the SOR method. The law of the wall is not used on the boundaries of the permeable groin that consists of a porous medium. Following the method that Michioku et al. (4) used, the shear stress on the boundary between open and porous medium sections is evaluated by the normal derivatives of the tangential velocity in the open section and the apparent tangential velocity in the porous medium section on the boundary.

CALCULATION CONDITIONS

Flume conditions of this study are set in accordance with those of the experiment by Michioku et al. (4), where flow structures around a rubble mound groin under non-overflow conditions are focused on. In particular, hydraulic settings and porous material characteristics follow those of case 3 in their experiment. The dimensions of the experiment flume are illustrated by Fig.1. Here, the dimensional and hydraulic settings are as follows: channel length, L = 15.0(m); channel width, B = 2.0(m); groin length, l_g = 1.0(m); groin width, b_g= 0.3(m); distance from the upstream end to the upstream side of the groin = 4.0(m); discharge = 0.0519(m^3/s); slope = 1/800; water depth at the upstream end, h_0 = 0.096(m); water depth at the downstream end = 0.037(m); and representative velocity at the upstream end, U_0 = 0.283(m/s). For settings of the porous medium, the diameter of rubble, d_m = 0.035(m), and the porosity of the groin, n = 0.38.

The parameters of numerical calculations are as follows; Smagorinsky coefficient, C_S = 0.1; and the coefficients representing the shapes of permeable material, e = 0.015, and f = 30.0.

The number of grid cells is 300*50*20 for downstream, cross-stream, and vertical directions, respectively. The calculation time step is set to 0.001(s), and the total number of calculation steps is 300,000. At the upstream end of the flume in the calculation, inflow velocity distributions and the water level are given. At the downstream cross-section of the flume, the water level is given, and the continuative condition, where normal derivatives of velocity components and pressure are 0, is applied.

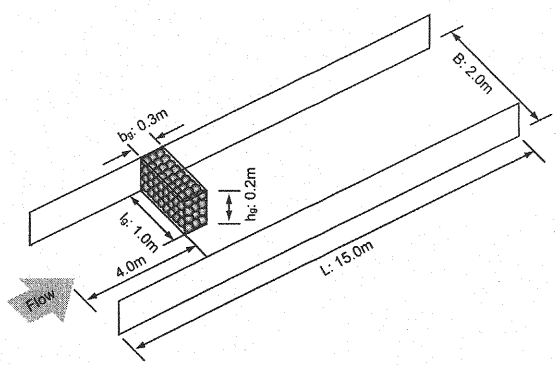

Fig. 1 Flume dimensions

COMPARISONS BETWEEN CALCULATION AND EXPERIMENT RESULTS

The applicability of the proposed model is evaluated by making a comparison between the exiting experiment (4) and the calculation results. This comparison is implemented for time- and depth-averaged results. Fig. 2 shows the comparison of the time-averaged water levels, Fig. 3 shows the time- and depth-averaged velocity vectors, and Fig. 4 shows the standardized (by U_0) time- and depth-averaged distributions of the downstream velocity component along the cross-stream axis at the point where locates at $x/h_0 = 4.0$ from the downstream end of the groin.

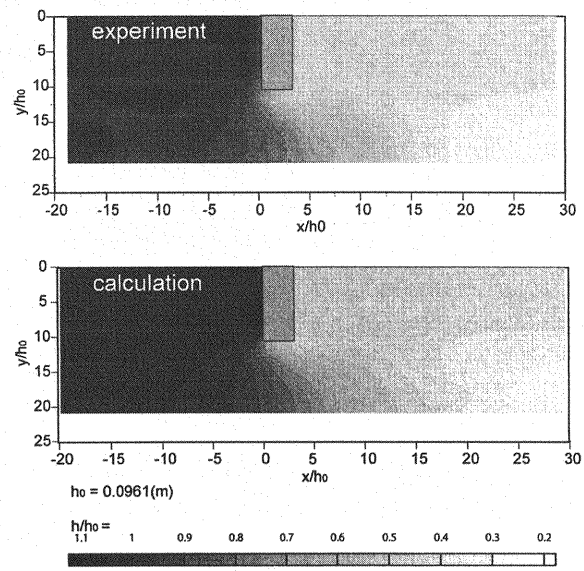

Fig. 2 Time-averaged water level (upper: experiment, lower: calculation)

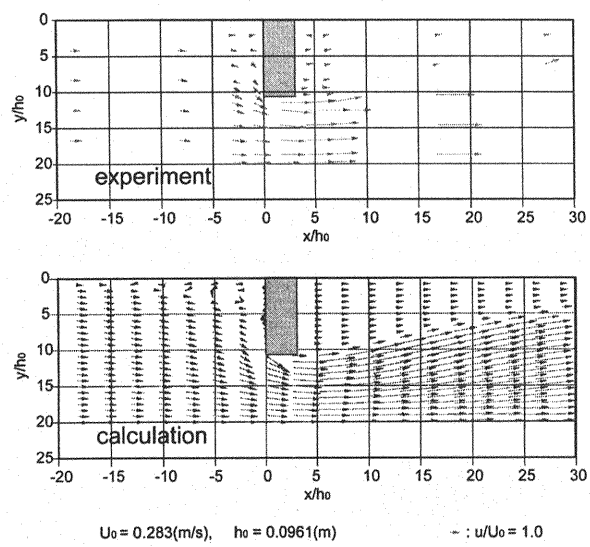

Fig. 3 Time- and depth-averaged velocity vectors (upper: experiment, lower: calculation)

These comparisons illustrate that the proposed numerical model show close agreement with experiment results. Hence, it is confirmed that the proposed model is sufficiently applicable for flows in a combined region of the open channel and the porous medium sections, when it is aimed at solving depth-averaged results. However, Fig. 4 shows some discrepancy between the experiment and the calculation results in regions where the experiment result has peaks of velocity. This suggests that the calculation results by the proposed model have a tendency to provide more spatially diffused distributions of physical values.

TEMPORAL RESULTS AND DISCUSSIONS

In the previous section we attempted to show the applicability of the proposed model for the time- and depth-averaged flows. From those results, it is assumed that the model is also able to provide the practical temporal solutions of the unsteady flows. In the following sections we will discuss the temporality and the three-dimensionality of flows based on this assumption.

An understanding of coherent structures of vortices is required when the three-dimensionality of flows needs to be described. Generally, qualitative evaluations of those coherent structures are performed by illustrating isosurfaces of vorticity in an objective region. However, several difficulties emerge when this method is applied in this study. One is that illustrating vorticity needs to fix the orientation of their defining axes. Their directions are not always the same as those of vortices' axes, and entire three-dimensional structures of vortices are hence not able to be figured. The other is that the predominance of mean shear stresses on the shear layer tends to hide small fluctuations of vorticity by temporal eddy structures. In this study, the shear layer between the main channel and the downstream section of the groin is strong, and this technique is thereby regarded as not being appropriate for capturing temporal structures of the vertical eddy cores in the shear layer. Here, the λ_2 method is employed instead of illustrating isosurfaces of vorticity. It is proposed by Jeong and Hussain (12). This technique is used to define cores of vortex structures, by assuming local pressure minimums exist in centers of rotational motions of flows. This method works well because, in the centers of large turbulent vortex structures, pressure is not generally in balance with the centrifugal force produced by rotational flow. This technique also removes isovorticity surfaces caused by near-fixed boundary shear.

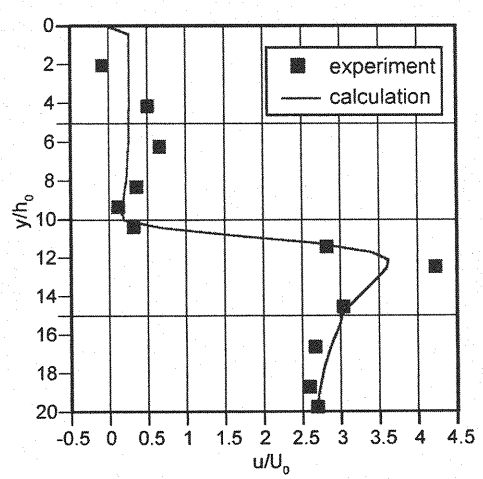

Fig. 4 Time- and depth-averaged downstream velocity distribution at $x/h_0 = 4.0$

Fig. 5 shows the temporal vortex core structures of the calculation result by illustrating the isosurfaces where λ_2 = -0.005 and velocity vectors of cross-section components. In this figure, capital letters denote locations of four major core structures: A) the lateral core of the vortex by the major secondary flow in the main channel in the constriction section; B) the lateral core by the minor counter-directional secondary flow that is generated from the downstream side of the groin; C) the vertical cores of the separated lateral eddies which are generated along the shear layer; and D) the vertical cores of the separated lateral eddies from the right bank of the channel. A close-up view of core A is shown in Fig. 6. The major secondary flow, represented by core A, is originally generated by the submerging flow at the upstream side of the groin, and has the counter-clockwise direction at the constriction section. The core structure of this secondary flow seems to remain in the downstream section from the constriction. However, velocity vectors show that the actual rotational flow in cross-sections converge more upstream than the end of the core. Fig. 7 shows a close-up view of cores B and C. One can observe that the minor secondary flow, represented by core B, has the counter direction (clockwise) to the major secondary flow, and the vertical cores of lateral eddies are separated from this minor secondary flow. Also, the separated vertical cores are connected to each other by the lateral cores that have the same rotational direction to the minor secondary flow in the down stream section from the point where cores are separated.

This visualization method is applied at each time step, and an animation is made by those images. This animation shows that the unsteady motions of each core structure are intermittent. However, the locations and the shapes of these structures do not change so much over time, except for the locations of vertical separation cores which are transported downstream. The structures of the cores beside the permeable groin are hence regarded as stable during the calculation.

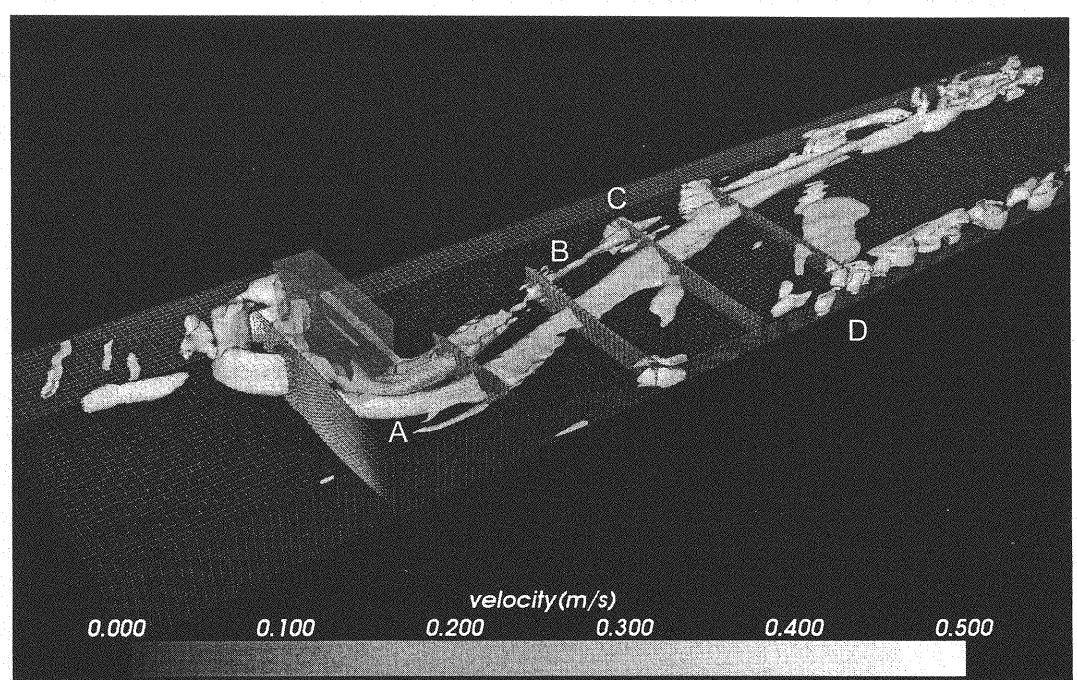

Fig. 5 Isosurfaces of λ_2 = -0.05 and velocity vectors on cross-section components (permeable)

Characteristics of these vortex cores around the permeable groin will be clearer when the result is compared to those of the vortex cores around the impermeable groin. Fig. 8 shows the vortex core structures of the calculation result of the flow around the impermeable groin, in which the same visualization method to Fig.5 is applied. In this calculation, the hydraulic conditions are the same as those for the case of the permeable groin. Although the types of elements of basic vortex structures, such as core A to D in Fig. 5, are identical, several differences can be easily observed. The secondary flows around the impermeable groin have much higher velocity than those around the permeable groin. In particular, the minor secondary flow that is generated on the left side of the major secondary flow is intensive compared to that of the permeable groin case. The other difference is that the vortex core structures in the case of the impermeable groin is much complex than that of the permeable groin case. This not only shows the spatial complexity, but also shows that of time-dependent characteristics. The animation of the same images in Fig. 8 shows that core structures of vortex in the down stream section of the impermeable groin are chaotic and very unsteady. This indicates that the large scale turbulence exists in the down stream section of the impermeable groin. Akahori find that the existence and the intermittency of secondary flows in a constriction section relates to the generation of lateral separation eddies in a downstream section of the constriction (5).

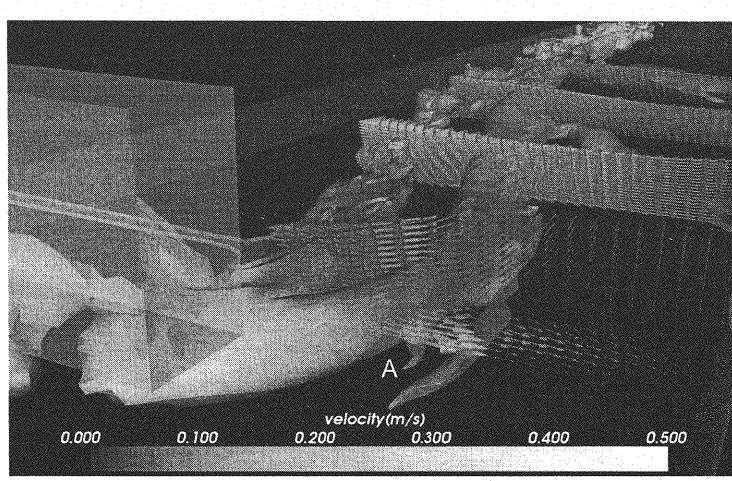

Fig. 6 Close-up view of core A in Fig. 5

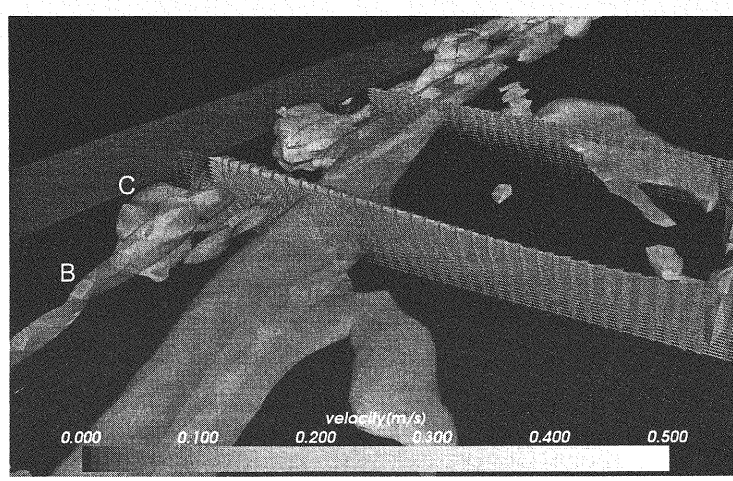

Fig. 7 Close-up view of cores B and C in Fig. 5

The results of this study may be relevant to the same context. The calculation results show that the strong turbulence is not observed in the downstream section of the permeable groin where the secondary flow is moderate, and the turbulence can be easily observed in the same section of the impermeable groin where the strong secondary flow exists. These results imply that the mechanism of the large scale turbulence generation varies according to the difference of the permeability of the groin material because of the difference of their characteristics to generate the secondary flows. The permeable groin may relax the pressure difference around itself, provide the moderate secondary flows, and restrain the generation of the lateral eddies which cause the large scale instability, in the right downstream section of the groin.

The result, in which the permeable groin may restrain the secondary flows and the large scale instability, does not confirm that the groin restrains every type of instability in different scales. The applicability of the proposed flow model with the non-Darcian resistance law for porous medium is then discussed, in terms of this difference of the scale of instability. The photographs of the temporal surface of the existing experiment (13) (shown by Photo. 6-7) show that small scale waves, which are not reproduced in the calculation results, emerge in the downstream of the dike, and those small waves implies the existence of the small scale turbulence structures that are not considered by the proposed model here. One of possible source that cause small scale turbulence in the downstream section of the dike is the turbulence of the flow in the porous of the dike. In porous medium, turbulence is treated as a kind of friction by the model. It is based on the considerations on time-averaged results, and the temporal sub-grid scale turbulence is not specifically modeled there, although the flows in the open section are solved with the conventional sub-grid scale model. Hence, we predicted that the proposed model cannot produce the small scale instability caused by temporal small turbulence structures in a porous medium. However, the problem is that such the small scale instability which is ignored in the process of the model's derivation may have influences on the generation of respectively large scale turbulence structures, which have to be resolved by the grid system in this numerical calculation case.

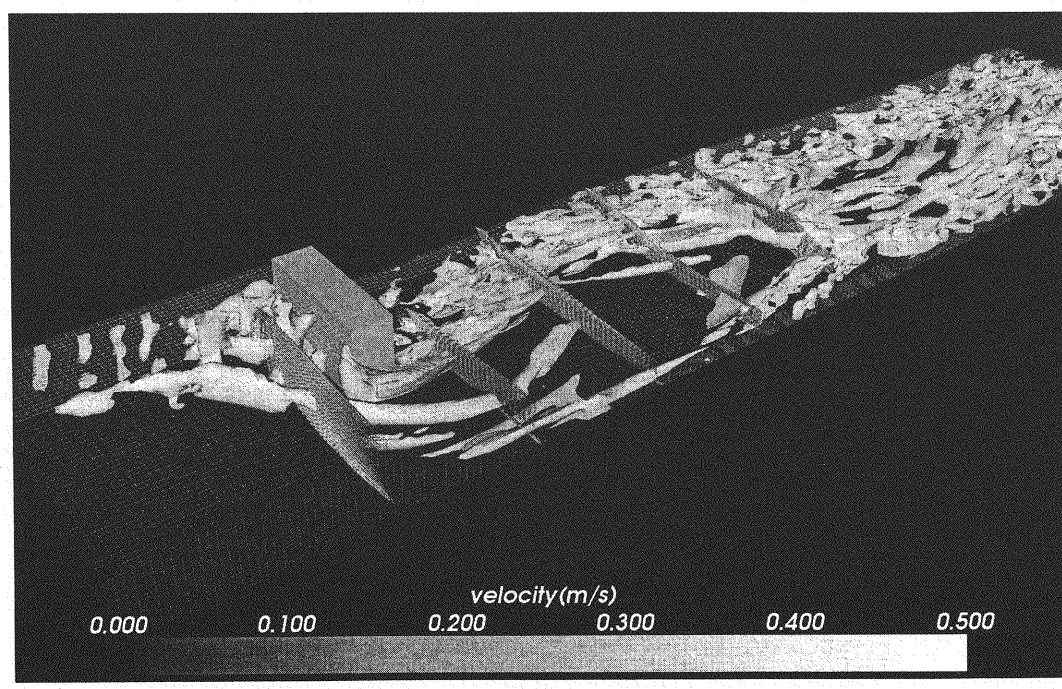

Fig. 8 Isosurfaces of λ_2 = -0.05 and velocity vectors on cross-section components (impermeable)

In order to approximate the influence of this small scale instability in the proposed numerical method and to investigate its importance, the instability is modeled by the normally distributed random noise based on the assumption that the instability by a permeable structure is unidirectional. The proposed noise is added on the normal velocity components on the first grid cells from the groin's wall at the downstream side. The value of the dispersion of the normally distributed noise is given by experimental results by Ujttewaal et al. (14) (Eq. 6).

$$\ln\left(\frac{\overline{u'^2}}{Uc^2}\right) = -1.3\ln\left(\frac{x_n}{D}\right) + b \qquad (6)$$

Here, U_c: actual flow velocity in porous medium, x_n: normal distance from a downstream wall, and b: intercept value given as –0.38. The effectiveness of this random noise modeling method of the small scale fluctuations caused by porous medium is examined by making a comparison of the calculation results between numerical models with and without the random noise component by Eq. 6. Fig. 9 shows the results by the model without the artificial noise and Fig. 10 shows that with the noise. A comparison of these figures illustrates that the ad hoc noise model increases the intensity of the turbulence in the open channel section without disturbing the distributed pattern of the turbulence.

However, this ad hoc random noise method is not yet sufficient to reproduce the turbulence of the expected intensity. Fig. 11 shows results of the numerical calculation with the impermeable groin case. In this tentative calculation, all the configurations are same as the previous cases with the permeable rubble mound groin, except for its permeability and that the random noise is not added on the velocity component for this impermeable case. Comparing Fig. 10 to Fig. 11, the turbulence intensity of the impermeable groin case is clearly higher than that of the ruble-mound groin case though the impermeable case does not have artificial methods to provide instability on the right downstream side of the groin. In this case, the turbulence in the downstream section of the groin is hence generated by the mean flow structures around the impermeable groin. The unpublished result of the existing experiment that is compared with the calculation results in this study shows that the maximum orders of the intensity of turbulence are not very different from the impermeable groin case and the rubble-mound groin case. This result suggests that the mechanism to generate turbulence in the right downstream section of the groin also exists in the case with permeable groin, and the simple ad hoc noise model cannot reproduce this mechanism. In the impermeable case, in which the mean flow structure is the dominant souse of turbulence, the model succeeds in creating turbulence in the same downstream section. Hence, it is supposed that the mechanism to generate turbulence in the downstream section of the permeable dike is not the mean flow structure, unlikely to the impermeable groin case. In a research paper written by Ujittewaal et al. (14), they reported that small scale instabilities that are generated by a permeable structure in a channel were merged and that they made large scale turbulence structures by this merging process. We assume that the same process occurs in the downstream section of the rubble-mound groin. A model including this merging process is required to reproduce the specific structured instability that will be self-organized to make the larger scale turbulence in a downstream. This contradicts the assumption of the simple ad hoc noise model that the instability by the permeable structure is unidirectional. The most accurate method of including the merging process of small scale instability without any contradiction is to resolve a calculation grid smaller than the scale of small instability by a porous medium (e.g. Kimura et al. (15), in which a grid system is precisely resolved around the square rods of a grid turbulence generator). However, in a non-hydrostatic three-dimensional numerical calculation, it is not yet practical to construct such a high resolution gird system because of its high cost of computing. In a future work, new methods that are able to reproduce such the merging process without such the demanding conditions are thereby required for more improved numerical calculations of flows around permeable structures.

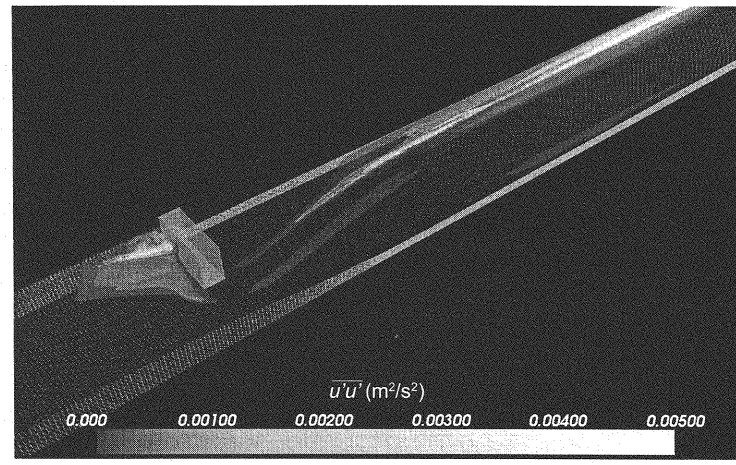

Fig. 9 Isosurfaces of magnitude of turbulence ($\overline{u'u'}$) (permeable groin WITHOUT noise model)

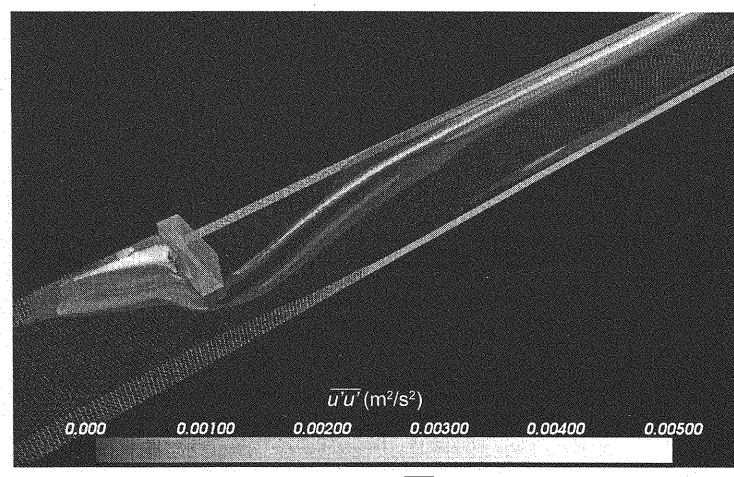

Fig. 10 Isosurfaces of magnitude of turbulence ($\overline{u'u'}$) (permeable groin WITH noise model)

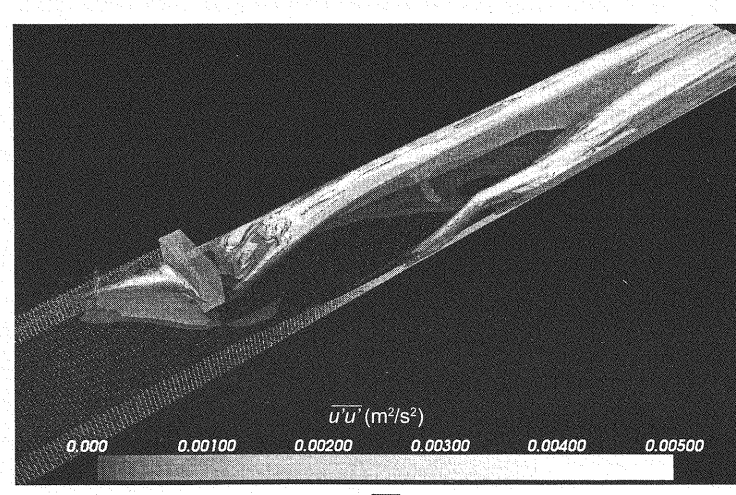

Fig. 11 Isosurfaces of magnitude of turbulence ($\overline{u'u'}$) (impermeable groin WITHOUT noise model)

CONCLUSIONS

In this study, we propose a three-dimensional numerical model, which is a combined model of the Large Eddy Simulation (LES) model for an open channel section and the non-Darcian porous flow model for a porous medium section. The model is applied to a numerical analysis of flows around a permeable groin that is a model of a rubble-mound groin, and flow mechanisms are investigated. The applicability of this model is also examined through this analysis. Conclusions of this study are summarized as follows.

1) The applicability of the proposed model to investigate general characteristics of flows around a rubble-mound groin is confirmed by a comparison between time- and depth-averaged calculation results and exiting experiment results.

2) A permeable groin reduces the intensity of secondary flows in the main channel section beside a groin, and thus restrains the generation of large scale lateral eddies, which are induced by secondary flows and cause large scale instability, in a shear layer.

3) The proposed model cannot rationally reproduce a merging process of small scale eddies generated by porous medium in a permeable groin in a right downstream section of the groin. The establishment of a model that can take into account this process is required in future work to perform more accurate numerical analyses.

REFERENCES

1. Maeno, S., Michioku, K., Ohnishi, T., and Morinaga, S. : Hydraulic characteristics in a failure stage of a rubble mound weir, Journal of Applied Mechanics, Vol.5, JSCE, Vol.5, pp.657-664, 2002 (in Japanese).
2. Maeno, S., Michioku, K., Morinaga, S., and Kikuchi, K. : Flow Analysis Around a Rubble Mound Weir, Annual Journal of Hydraulic Engineering, Vol.48, pp.829-834, 2004 (in Japanese).
3. Michioku, K., Maeno, S., Haneda, M., Yoshizawa, T. : Analysis on Discharge over and through a Rubble-mound Weir, Journal of Hydraulic, Coastal and Environmental Engineering, No.740/II-64, JSCE, pp.131-142, 2003 (in Japanese).
4. Michioku, K., Nanjo, M., Ishigaki, T., and Maeno, S. : Hydrodynamics, Journal of Hydraulic, Coastal and Environmental Engineering , No.782/II-70, JSCE, pp.31-50, 2005 (in Japanese).
5. Akahori, R.: Modeling sediment transport in eddy recirculation zones of the Colorado River in Grand Canyon, PhD dissertation, Arizona State University, 2007.
6. Nagata, N., Hosoda, T., Muramoto, Y. and Nakato, T. : Analysis of Local Scour around a Spur Dike using 3-D Mathematical Model Developed with Moving-grid System and Nonequilibrium Sediment-transport Theory, Journal of Hydraulic, Coastal and Environmental Engineering , No.684/II-56, JSCE, pp.21-34, 2001 (in Japanese).
7. Ushijima, S., Fukutani, A., Yoshikawa, N., and Nezu, I. : Numerical Prediction for collapse of Permeable Dam due to Overflows with 3D Multiphase-flow Solver (3D MICS), Annual Journal of Hydraulic Engineering, Vol.50, pp.841-846, 2006 (in Japanese).
8. Deardorff, J. W.: A numerical study of three-dimensional turbulent channel flow at large Reynolds numbers, Journal of Fluid Mechanics, 41(2), pp.453-480, 1970.
9. Hosoda, T., Nagata, N. & Muramoto, Y. 1996. Numerical analysis of unsteady open channel flows by means of mov-ing boundary fitted coordinate system. Journal of Hydraulic, Coastal and Environmental Engineering, No.533/II-34, JSCE, pp.267-272, 1996 (in Japanese).
10. Ward, J. C.: Turbulent flows in porous media, Journal of Hydraulic Engineeering, ASCE, Vol.90, HY5, pp.1-12, 1964.

11. Yabe, T. and Aoki, T.: A universal solver for hyperbolic equations by cubicpolynomial interpolation I. One-dimensional solver, Comp. Phys. Comm. 66, pp. 219-232, 1991.
12. Jeong, Jinhee., and Hussain, Fazle, On the identification of a vortex. J. Fluid. Mech., 285, pp.69-94, 1995.
13. Michioku、K., Ishigaki、K., Maeno、S., Takehara、K., Etoh, T., Nanjo, M., and Haneda, M.. : Hydrodynamic Properties of Rubble Mound Weir and Groin Installed in an Open Channel, Annuals of Disas. Prev. Res. Inst., Kyoto Univ., No. 47 B, pp.581-600, 2004 (in Japanese).
14. Ujittewaal, W. S. J. and Jirka, G. H.: Grid turbulence in shallow flows, J. Fluid Mech., Vol.489, pp.325-344, 2003.
15. Kimura, I., Ujittewaal, W.S.J., and Hosoda, T. : Computation of Shallow Grid Turbulence using 2D and 3D RANS Models. Annual Journal of Hydraulic Engineering, Vol.51, pp.799-804, 2007 (in Japanese).

APPENDIX – NOTATION

The following symbols are used in this paper:

i = representing each component of grid system;

u_i = flow velocity;

x_i = axes of the grid system;

t = time;

ρ = fluid density;

g_i = body force;

ν = eddy viscosity;

C_S = Smagorinsky coefficient;

Δ = $(\Delta x_1 \Delta x_2 \Delta x_3)^{1/3}$;

Δx_i = grid scale;

P = $p+2/3q$;

p = pressure;

q = SGS kinetic energy;

H = water level;

u, v = horizontal components of flow velocity;

w = vertical component of flow velocity;

x, y = horizontal component of the cartesian coordinate system;

U_s = apparent velocity;

u_{si} = nu_i;

n = porosity;

U = ensemble averaged velocity;

u' = fluctuating value form the ensemble averaged value;

K = characteristic parameters of porous medium;

c = characteristic parameters of porous medium;

d_m = average diameter of particles of porous medium;

e = non-dimensionalized coefficient of particle shape;

f = non-dimensionalized coefficient of particle shape;

L = channel length;

B = channel width;

l_g = groin length;

b_g = groin width;

U_0 = representative velocity at the upstream end;

U_c = actual flow velocity in porous medium;

x_n = normal distance from a porous wall; and

b = intercept value.

(Received Aug 06, 2008 ; revised Jan 29, 2009)